

Article

Evaluation of Fe²⁺/Peracetic Acid to Degrade Three Typical Refractory Pollutants of Textile Wastewater

Jiali Yu ^{1,†}, Shihu Shu ^{1,†}, Qiongfang Wang ², Naiyun Gao ³ and Yanping Zhu ^{1,*}

¹ College of Environmental Science and Engineering, Donghua University, Shanghai 201620, China; gloria11071219@163.com (J.Y.); shushihu@dhu.edu.cn (S.S.)

² College of Chemistry and Chemical Engineering, Shanghai University of Engineering Science, Shanghai 201600, China; wqfang2010@126.com

³ State Key Laboratory of Pollution Control Reuse, Tongji University, Shanghai 200092, China; gaonaiyun@126.com

* Correspondence: yanpingzhu@dhu.edu.cn

† These authors contributed equally to this work.

Abstract: In this work, the degradation performance of Fe²⁺/PAA/H₂O₂ on three typical pollutants (reactive black 5, ANL, and PVA) in textile wastewater was investigated in comparison with Fe²⁺/H₂O₂. Therein, Fe²⁺/PAA/H₂O₂ had a high removal on RB5 (99%) mainly owing to the contribution of peroxy radicals and/or Fe(IV). Fe²⁺/H₂O₂ showed a relatively high removal on PVA (28%) mainly resulting from ·OH. Fe²⁺/PAA/H₂O₂ and Fe²⁺/H₂O₂ showed comparative removals on ANL. Additionally, Fe²⁺/PAA/H₂O₂ was more sensitive to pH than Fe²⁺/H₂O₂. The coexisting anions (20–2000 mg/L) showed inhibition on their removals and followed an order of HCO₃[−] > SO₄^{2−} > Cl[−]. Humic acid (5 and 10 mg C/L) posed notable inhibition on their removals following an order of reactive black 5 (RB5) > ANL > PVA. In practical wastewater effluent, PVA removal was dramatically inhibited by 88%. Bioluminescent bacteria test results suggested that the toxicity of Fe²⁺/PAA/H₂O₂ treated systems was lower than that of Fe²⁺/H₂O₂. RB5 degradation had three possible pathways with the proposed mechanisms of hydroxylation, dehydrogenation, and demethylation. The results may favor the performance evaluation of Fe²⁺/PAA/H₂O₂ in the advanced treatment of textile wastewater.

Keywords: peracetic acid; advanced oxidation; reactive dyes; aniline; polyvinyl alcohol



Citation: Yu, J.; Shu, S.; Wang, Q.; Gao, N.; Zhu, Y. Evaluation of Fe²⁺/Peracetic Acid to Degrade Three Typical Refractory Pollutants of Textile Wastewater. *Catalysts* **2022**, *12*, 684. <https://doi.org/10.3390/catal12070684>

Academic Editors: Hao Xu and Yanbiao Liu

Received: 28 May 2022

Accepted: 14 June 2022

Published: 22 June 2022

Publisher's Note: MDPI stays neutral with regard to jurisdictional claims in published maps and institutional affiliations.



Copyright: © 2022 by the authors. Licensee MDPI, Basel, Switzerland. This article is an open access article distributed under the terms and conditions of the Creative Commons Attribution (CC BY) license (<https://creativecommons.org/licenses/by/4.0/>).

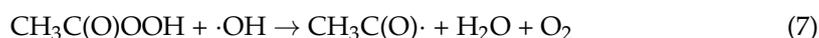
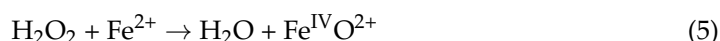
1. Introduction

The textile industry was one of the most water-consuming and key industrial branches, especially in developing countries. In China, the amount of textile wastewater, around 80% of which is from the printing and dyeing process [1], ranked third among all the 41 industries and accounted for 10.1% [2]. Generally, the discharged textile wastewater was treated either by on-site treatment plants in the factory or a combination of factories and urban wastewater treatment plants (WWTPs) to meet the wastewater discharge standard. However, the increasingly stringent discharge standard forces the advanced tertiary treatment urgent for the enhanced removal of refractory pollutants.

Reactive dyes, aniline (ANL), and polyvinyl alcohol (PVA) are three types of typical refractory pollutants in printing and dyeing wastewater and are of increasing environmental concern [3]. Reactive dye is the most important dyeing class for cellulosic fibers [4], up to 10–50% of which would flow into wastewater in the dyeing process [5]. ANL is an important intermediate in syntheses of benzidine azo dyes [2] as well as a product derived from the biotransformation of azo dyes [6]. ANL has been listed as a priority pollutant by the Environmental Protection Agency of the United States due to its carcinogenic and mutagenic effects [7]. In the latest amended Discharge Standard of Water Pollutants for Dyeing and Finishing of Textile Industry (GB 4287-2012) in China [8], the discharge limit

of ANLs was regulated as undetected, which was actually difficult for factories to meet at affordable expenses. PVA, a water-soluble refractory polymer, is widely used in the sizing process of cotton blended fabrics and was lost to the effluent during the desizing process [9]. The discharge of PVA may deteriorate the receiving body of water via causing the lack of dissolved oxygen in the aquatic environment and the release of harmful metals from the sediment [10]. The removal of PVA via the conventional biological process was challenging due to its poor biodegradability [11].

The advanced oxidation process (AOP) is widely adopted as the tertiary treatment for the removal of low-level refractory organic pollutants from the secondary effluent of industrial textile wastewater [12–19]. Recently, Fe^{2+} /peracetic acid (PAA) has emerged as a potential alternative to the conventional Fe^{2+} /hydrogen peroxide (H_2O_2) Fenton AOP [20,21]. PAA has a high disinfection efficiency and less formation of harmful disinfection byproducts (DBPs) compared to those chlorine-based disinfectants [22]. Thus, it is recommended as an attractive disinfectant for secondary and tertiary wastewater effluents in many countries, (e.g., Canada and parts of Europe) [23–25]. In fact, the PAA solution is an equilibrium mixture of PAA, H_2O_2 , and acetic acid [26], and the PAA-based Fenton system was defined as Fe^{2+} /PAA/ H_2O_2 . During the Fe^{2+} /PAA/ H_2O_2 process, PAA played a key role within the initial 5 s and H_2O_2 became the dominant oxidant afterward due to the much higher reaction rate of PAA with Fe^{2+} (>650 times) compared to that of H_2O_2 [27]. Activation of PAA by Fe^{2+} may primarily generate $\cdot\text{OH}$, $\text{CH}_3\text{C}(\text{O})\text{O}\cdot$, and $\text{Fe}(\text{IV})$ according to reactions (1–5) [27,28]. Moreover, $\cdot\text{OH}$ would also react with PAA and H_2O_2 to generate secondary radicals, (e.g., $\text{CH}_3\text{C}(\text{O})\cdot$, $\text{CH}_3\text{C}(\text{O})\text{OO}\cdot$, and $\text{HO}_2\cdot$) via reactions (6–9), and the reaction rate of $\cdot\text{OH}$ with PAA was much higher compared with H_2O_2 [27,29]. That said, the proportion of PAA and H_2O_2 would affect the distribution of organic radicals and $\cdot\text{OH}$ in the Fe^{2+} /PAA/ H_2O_2 process. In previous research [30–33], PAA-based AOP has exhibited structural selectivity in the removal performance of target pollutants and shown comparable or even superior performance compared to H_2O_2 -based AOP.



Among the studies about the active dye degradation by PAA-based AOPs, H_2O_2 and PAA-related organic radicals played dominant roles in the removal of methyl blue and Brilliant Red X-3B, respectively [21,34]. Co(II)-mediated PAA oxidation in previous work has shown a minor contribution of $\text{CH}_3\text{C}(\text{O})\text{OO}\cdot$ to the degradation of ANL [30]. In addition, the degradation of PVA has been evaluated mainly in H_2O_2 -based AOPs with the reaction rate constant of PVA with $\cdot\text{OH}$ in the order of 10^6 – 10^7 $\text{M}^{-1}\text{s}^{-1}$ [35], while scarcely in PAA-based AOP. Considering the different structural characteristics of the three typical pollutants, there is a need to comparatively evaluate their degradation efficacies by Fe^{2+} /PAA/ H_2O_2 and assess the contributions of radicals produced, respectively, by PAA and H_2O_2 .

The objectives of this study are to investigate: (1) the effectiveness of Fe^{2+} /PAA/ H_2O_2 to degrade reactive black 5 (RB5), ANL, and PVA in comparison to Fe^{2+} / H_2O_2 ; (2) the impact of operating conditions, (i.e., Fe^{2+} and PAA dosages, coexisting ions and natural

organic matter); (3) contributions of $\cdot\text{OH}$ and PAA-related radicals in their degradation under different pH conditions; (4) the acute toxicity alteration during the process; and (5) degradation intermediates and possible pathways. The main novelty of this work is to investigate the relationship between $\text{Fe}^{2+}/\text{PAA}/\text{H}_2\text{O}_2$ and pollutant structure, obtaining the applicability of the process in textile water treatment.

2. Materials and Methods

2.1. Chemicals and Materials

RB5, ANL, sodium thiosulfate, potassium iodide, acetic acid, ferrous sulfate ($\text{FeSO}_4 \cdot 7\text{H}_2\text{O}$), phosphoric acid, sodium chloride, and sodium sulfate were of analytical grade and obtained from Shanghai Titan Scientific Co., Ltd. (Shanghai, China). Ammonium molybdate ($(\text{NH}_4)_2\text{MoO}_4$), sodium hydroxide (NaOH), sulfuric acid, and *p*-chlorobenzoic acid (*p*CBAs) were purchased from Sinopharm Chemical Reagent Co. (Shanghai, China). Tert-butanol (TBA), methanol (MeOH), and 5,5-dimethyl-1-pyrroline N-oxide (DMPO) were of chromatographic grade and purchased from Fisher Scientific (Fair Lawn, NJ, USA). H_2O_2 (30%, w.t.) solution, PVA (Type 1788) with an average molecular weight of 46,000 g/mol (hydrolysis degree of 88%), humic acid (HA), N, N-Diethyl-*p*-phenylenediamine (DPD), and 5,5-dimethyl-1-pyrroline N-oxide (DMPO) were purchased from Sigma-Aldrich (Shanghai, China). All solutions were prepared with ultrapure water from a Millipore Milli-Q water system (Direct-Q3 UV). The secondary effluent taken from a municipal wastewater treatment plant (Songjiang District, Shanghai, China) was used as the real wastewater with dissolved organic carbon (DOC) of around 4.5 mg C/L after filtered through a 0.45 μm membrane. PAA solution, containing PAA: H_2O_2 at a molar ratio of 1.34:1, was freshly prepared according to the reaction (Equation (10)) and stored at 4 °C [36].



2.2. Experimental Procedures

All experiments were conducted in a 200 mL glass reactor with constant magnetic stirring at room temperature (20 ± 1 °C). The reaction solution contained designated concentrations of target pollutants, the initial pH of which was adjusted to 3.0, 4.0, 5.0, 6.0, and 7.0 by sodium hydroxide (1 M) or sulfuric acid (1 M). Reactions were initiated by adding different dosages of PAA and $\text{FeSO}_4 \cdot 7\text{H}_2\text{O}$ simultaneously. Samples (1–2.5 mL) were withdrawn within 10 min at predetermined intervals and immediately quenched by excessive sodium thiosulfate ($[\text{Na}_2\text{S}_2\text{O}_3]/[\text{PAA}]_0$ molar ratio >10) for the analysis of target compounds. Meanwhile, PAA decay was also monitored by taking samples periodically without adding any quenching agent. To explore the contribution of direct PAA oxidation and the radicals produced from H_2O_2 contained in PAA solution, additional trials were also conducted by adding PAA only or $\text{Fe}^{2+}/\text{H}_2\text{O}_2$ (H_2O_2 dosage equal to the concentration of H_2O_2 in PAA solution). Quenching tests were performed by spiking 100 mM TBA or MeOH to the reaction solution before the addition of PAA and Fe^{2+} . The concentrations of TBA or MeOH were high enough to quench reactive radicals. To quantify the steady-state concentration of $\cdot\text{OH}$ in $\text{Fe}^{2+}/\text{PAA}/\text{H}_2\text{O}_2$ system under different pH conditions, the $\cdot\text{OH}$ probe (*p*CBAs) was spiked to the reaction solution and its time-dependent degradation was also analyzed.

The effect of water matrices on the degradation of the three target pollutants in $\text{Fe}^{2+}/\text{PAA}/\text{H}_2\text{O}_2$ system was assessed by adding Cl^- (0–2000 mg/L), SO_4^{2-} (0–2000 mg/L), HCO_3^- (0–2000 mg/L), and HA (0–10 mg C/L), respectively, to the reaction solution. The degradation tests were also conducted in practical wastewater effluent. Samples were also taken for oxidized products or DOC analysis at the beginning and end of each test. All experiments were conducted at least in duplicate, and the error bars represented the standard deviation.

2.3. Analytical Methods

The ANL and *p*CBA concentrations were measured by high-performance liquid chromatography (HPLC, Thermo Scientific UltiMate DioNEX 300, Waltham, MA, USA) coupled with a Symmetry-C18 column (5 μ m, 4.6 mm \times 250 mm) and a UV detector. The mobile phase for ANL was a 65:35 (*v/v*) mixture of methanol and ultrapure water at a flow rate of 1 mL/min. The mobile phase for *p*CBA was a mixture of methanol and phosphoric acid (70:30, *v/v* %) with a flow rate of 1 mL/min. The injection volumes of ANL and *p*CBA samples were 10 and 100 μ L, respectively. Both ANL and *p*CBA were analyzed at the wavelength of 230 nm. The RB5 concentration was measured with an ultraviolet spectrophotometer (UV1800) at a wavelength of 598 nm. The PVA concentration was measured using the modified colorimetric method [37]. Briefly, eight 25 mL volumetric flasks were prepared with each containing either 0, 0.05, 0.1, 0.2, 0.3, 0.4, 0.5, and 0.6 mL of 0.5 g/L standard PVA solution and diluted to 10 mL. Then, 5 mL of 4% boric acid and 2 mL of I₂-KI (1.27 g/L I₂ and 25 g/L of KI) were added. After equilibration for 5 min, the solutions were diluted to 25 mL and measured at a wavelength of 690 nm.

Electron paramagnetic resonance (EPR, EMXnano231, Bruker, Rheinstetten, Germany) was used to determine the reactive species with DMPO as the spin trapping agent, with further details presented in SI. The oxidized products of RB5 by Fe²⁺/PAA/H₂O₂ system were analyzed by HPLC-MS (Q Exactive Focus, Thermo Fisher Scientific, Waltham, MA, USA), and ANL was detected by GC-MS (Thermo Fisher Scientific, Waltham, MA, USA), the details of which were provided in SI. The PAA stock solution was regularly calibrated using titration method [7]. Concentrations of PAA and H₂O₂ in PAA solution were determined according to the Hach DPD method [38]. H₂O₂ concentration in the absence of PAA was measured using a triiodide absorbance method [39]. Acute ecotoxicity was assessed by the change of bioluminescence intensity bioluminescent with *Vibrio fischeri* bacteria in toxicity analyzer (HACH, Ames, IA, USA) [40], with the details of the method given in Supplementary Materials.

3. Results and Discussions

3.1. Process Degradation Efficiency Assessment

The degradation behaviors of Fe²⁺/PAA/H₂O₂ towards the three pollutants were comparatively evaluated at initial pHs of 3.0, 4.0, 5.0, 6.0, and 7.0 compared with PAA only and Fe²⁺/H₂O₂. As shown in Figure 1a, 90% of RB5 was removed through an initial fast degradation (94%) within 5 s, followed by a slow degradation in the Fe²⁺/PAA/H₂O₂ system, while a minor RB5 degradation (<5%) occurred in PAA only system due to the slow reaction rate. In the Fe²⁺/H₂O₂ system, RB5 removal decreased by 6% in the first 5 s and 75% in the whole process compared with Fe²⁺/PAA/H₂O₂, attributed to reactive oxidative species (ROS) generated from PAA in addition to H₂O₂. By contrast, ANL removal in the Fe²⁺/PAA/H₂O₂ system (47%) was comparable to that (39%) in the Fe²⁺/H₂O₂ system, which suggested that the degradation efficiency of ANL in the former was mainly attributed to the presence of H₂O₂ other than PAA. Interestingly, the PVA degradation efficiency was lower in the Fe²⁺/PAA/H₂O₂ system compared with the Fe²⁺/H₂O₂ system. This was likely because PAA reacted much faster with Fe²⁺ than H₂O₂ and thus contributed to its preferential consumption of Fe²⁺. On the other hand, the presence of PAA may convert \cdot OH to C \cdot via the reaction of \cdot OH with PAA according to Equation (10). In comparison with previously reported results (Table 1), this process showed a relatively rapid removal of these three pollutants, especially RB5 [41–46].

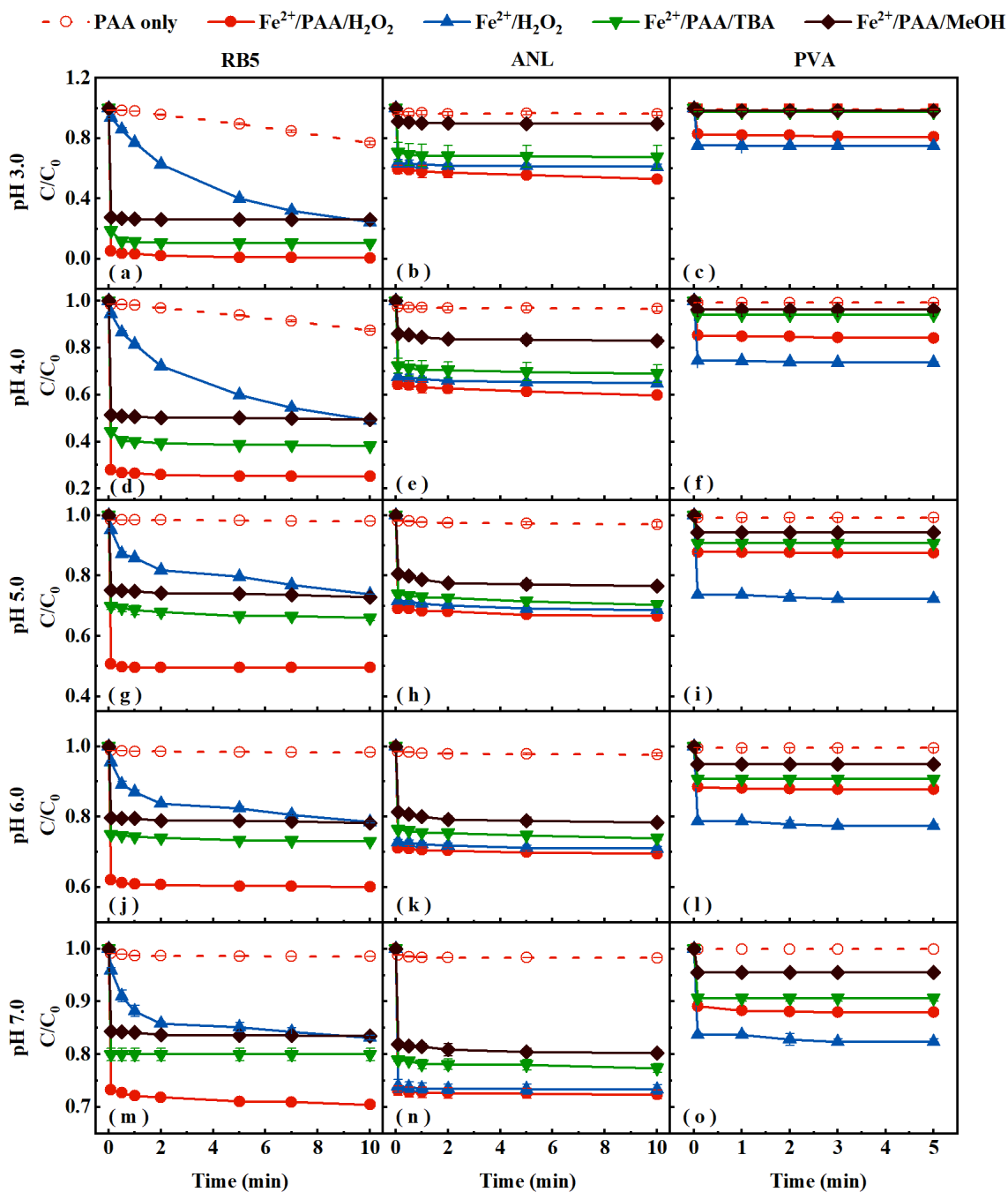


Figure 1. Time-dependent degradation of (a,d,g,j,m) RB5, (b,e,h,k,n) PVA and (c,f,i,l,o) ANL by different processes in a pH range of 3.0–7.0. Conditions: [PAA]₀ = 15 mg/L, [H₂O₂]₀ = 5 mg/L, [RB5]₀ = 20 mg/L, [PVA]₀ or [ANL]₀ = 10 mg/L, initial pH = 3.0, 5.0, and 7.0, T = 21 ± 1 °C.

Table 1. Comparison of different AOPs in removing RB5, ANL, and PVA with Fe²⁺/PAA/H₂O₂ system.

AOPs	Pollutants	Pollutant Concentration (mg/L)	Reaction Time (min)	Initial pH	Catalyst Dose (mg/L)	Oxidant Dose	Removal Efficiency (%)	References
Ag ₃ PO ₄ /Visible light	RB5	50	120	11.0	500	150 W	91	[41]
O ₃ /Co-Ce-O	RB5	100	80	7.0	1000	60 LPH	96	[42]

Table 1. Cont.

AOPs	Pollutants	Pollutant Concentration (mg/L)	Reaction Time (min)	Initial pH	Catalyst Dose (mg/L)	Oxidant Dose	Removal Efficiency (%)	References
Fe ₃ O ₄ /PMS	RB5	50	60	7.0	250	614.76 mg/L	94.86	[43]
AmGO/UV-A	RB5	100	120	8.0	5000	40 W	75	[44]
Fe ²⁺ /PAA/H ₂ O ₂	RB5	20	10	3.0	1.1	15/5 mg/L	94	This work
	ANL	10	10	3.0	2.2		47	
	PVA	10	5	3.0	2.2		20	
UV/SPC	ANL	93.13	120	6.8	314	17.85 mw/cm ²	54.25	[45]
UV/NiFe ₂ O ₄	PVA	25	140	6.0	300	15 W	94.3	[46]

Note: PS, persulfate; PMS, peroxymonosulfate; AmGO, amino-Fe₃O₄-functionalized graphene oxide; SPC, sodium percarbonate; LPH, Litres per hour.

The ·OH was identified in Fe²⁺/PAA/H₂O₂ system via EPR. Figure S1 showed that the characteristic peak of the DMPO-HO· spin adduct signal appeared in the spectrum, suggesting the existence of ·OH in the system. To differentiate between the contributions of ·OH and other ROSs, (i.e., peroxy radicals and Fe(IV)), TBA was used to quench ·OH ($k_{\text{OH/TBA}} = (3.8\text{--}7.6) \times 10^8 \text{ M}^{-1}\text{s}^{-1}$) [47], and MeOH was used as a quencher for both ·OH ($k_{\text{OH/MeOH}} = 9.16 \times 10^9 \text{ M}^{-1}\text{s}^{-1}$) [48] and acetyl(per)oxyl radicals, (i.e., CH₃COO· and CH₃C(O)OO·) [30]. As shown in Figure 1a–c, TBA significantly inhibited the removal of ANL and PVA by 15% and 17%, respectively, but showed negligible influence on RB5 removal. By contrast, MeOH inhibited the removal of RB5, ANL, and PVA by 25%, 37%, and 17%, respectively. These results further indicated that PVA degradation mainly depended on ·OH, ANL mainly on both ·OH and other ROSs, while RB5 was mainly on other ROSs compared to ·OH.

The influence of pH on the degradation of these three pollutants was investigated in a range of 3.0–7.0. Figure 1 showed that their degradation efficiencies declined with the increase in pH, the extent of which followed an order of RB5 > ANL > PVA. The pH effects for RB5 and PVA were more significant in Fe²⁺/PAA/H₂O₂ compared with Fe²⁺/H₂O₂, while similar for ANL. These results indicated that other ROSs were more susceptible to pH than ·OH, likely due to the higher reaction rate constants in Equations (1)–(3) (16,000–110,000 M⁻¹ S⁻¹) compared with Equations (4) and (5) (63–76 M⁻¹ S⁻¹) [27]. Therein, the former could be inhibited more significantly at the elevated pH mainly because of the higher OH⁻ concentration. Meanwhile, the higher pH could result in a decline in Fe²⁺ according to reaction 11.



3.2. Effects of PAA and Fe²⁺ Dosages on Pollutants' Removal

The effects of PAA and Fe dosages on the degradation efficiencies of the three pollutants were evaluated. As shown in Figure 2a–c, their removals increased with the PAA dosage rising from 5 to 15 mg/L likely attributed to the increased number of radicals. As the PAA dosage further rose to 30 mg/L, their removals either remained stable (RB5) or decreased, which may be explained by the quenching effect of PAA and/or H₂O₂ on radicals [30]. These results indicated that the optimal PAA dosage was 15 mg/L.

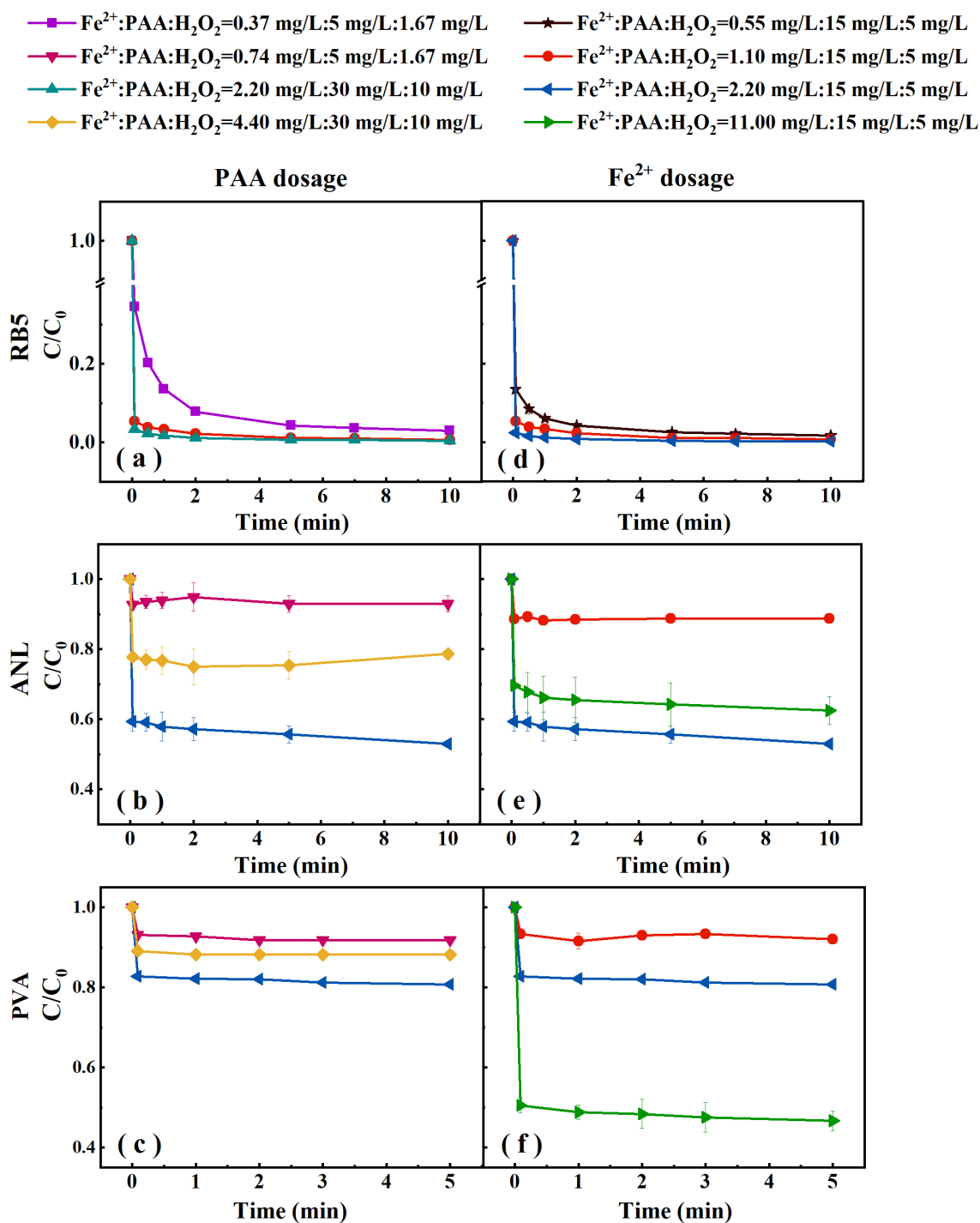


Figure 2. Effects of PAA and Fe²⁺ dosages on the degradation of (a,d) RB5, (b,e) ANL and (c,f) PVA. Conditions: [RB5]₀ = 20 mg/L, [PVA]₀ and [ANL]₀ = 10 mg/L, initial pH = 3.0, T = 21 ± 1 °C.

Moreover, the influence of Fe²⁺ dosage on their removals was studied with the PAA dosage of 15 mg/L. Figure 2d–f showed that RB5 removal was relatively stable against Fe²⁺ dosage from 0.55 to 2.20 mg/L, likely owing to the sufficient Fe²⁺ even at a low dosage (0.55 mg/L) for the activation of PAA/H₂O₂. ANL removal increased from 11% to 38% with the elevated Fe²⁺ dosage, implying the enhanced activation of Fe²⁺ on PAA/H₂O₂. While PVA removal increased initially (Fe dosage < 2.20 mg/L) and then remained unchanged. These results demonstrated that the dosages of both Fe²⁺ and PAA/H₂O₂ had a significant influence on the removal of these pollutants.

3.3. Effects of Coexisting Inorganic Anions and Humic Acid on Pollutants' Removal

3.3.1. Effects of Coexisting SO_4^{2-} , Cl^- , and HCO_3^-

Considering that textile wastewater generally had high contents of SO_4^{2-} , Cl^- , and HCO_3^- , their effects on the removal of the three pollutants were investigated with the anions' concentrations of 0–2000 mg/L. Figure 3 demonstrated that all these anions inhibited their removals, the extent of which followed an order of $\text{HCO}_3^- > \text{SO}_4^{2-} > \text{Cl}^-$. The inhibition of HCO_3^- was probably because of the quenching effect of HCO_3^- on $\cdot\text{OH}$ to generate less reactive $\text{HCO}_3\cdot$ according to reaction (12) with a high reaction rate constant ($>10^8 \text{ M}^{-1}\text{s}^{-1}$) [49]. In addition, HCO_3^- may consume Fe^{2+} to form nonreactive $\text{Fe}^{2+}\text{-HCO}_3^-$ complexes [20], and probably cause a pH increase simultaneously. Among these three pollutants, PVA was the most sensitive against these anions, indicating the possibly easier quenching of $\cdot\text{OH}$ by these anions than other ROSs. As for RB5, SO_4^{2-} at 2000 mg/L or HCO_3^- at 200 and 2000 mg/L significantly decreased the removals from 98 to 82.5% or from 98.6 to approximately 81.2%, respectively. The inhibition of SO_4^{2-} and Cl^- was likely because they could convert $\cdot\text{OH}$ and peroxy radicals to $\text{SO}_4\cdot^-$ and chlorine-containing radicals which may show relatively weak oxidative capacity towards these pollutants [36].

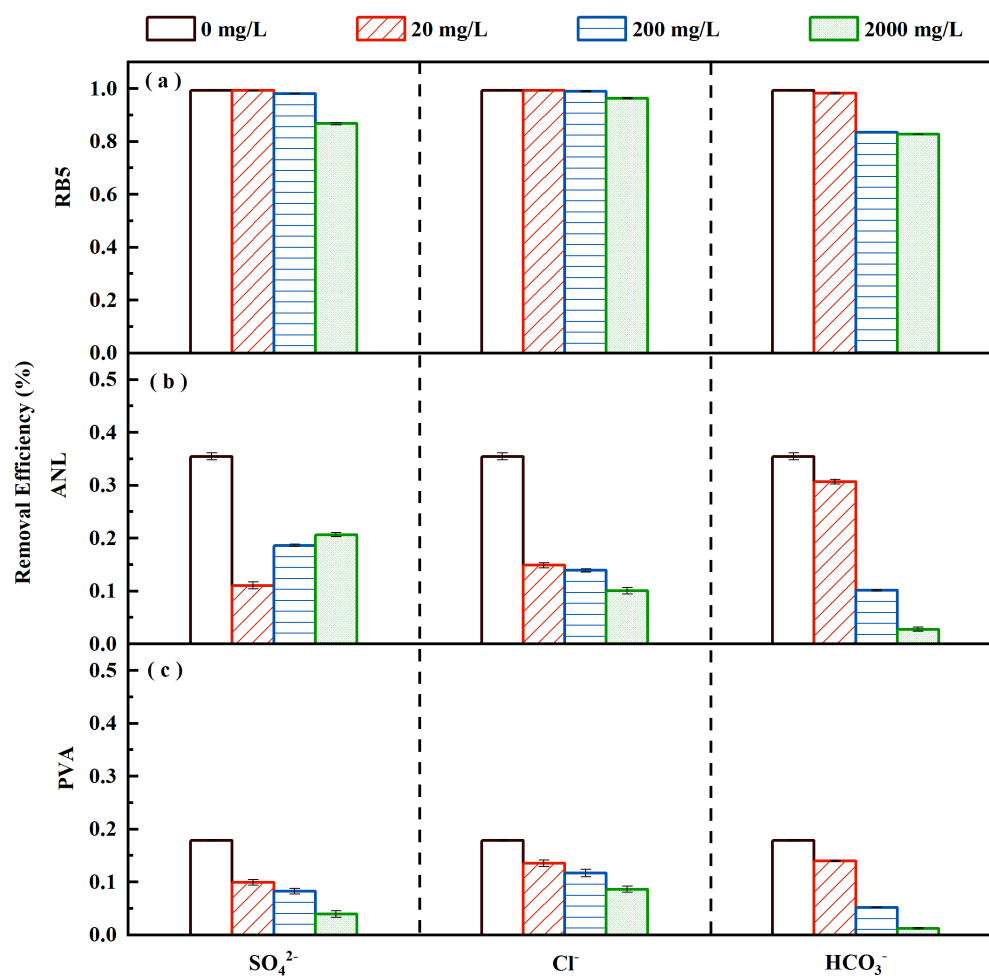
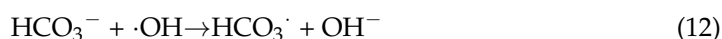


Figure 3. Effect of coexisting SO_4^{2-} , Cl^- , and HCO_3^- on the degradation of (a) RB5, (b) ANL, and (c) PVA in $\text{Fe}^{2+}/\text{PAA}/\text{H}_2\text{O}_2$ system. Conditions: $[\text{PAA}] = 15 \text{ mg/L}$, $[\text{RB5}]_0 = 20 \text{ mg/L}$, $[\text{PVA}]_0$ or $[\text{ANL}]_0 = 10 \text{ mg/L}$, $\text{pH} = 3.0$, $T = 21 \pm 1 \text{ }^\circ\text{C}$, $[\text{anion}] = 0, 20, 200, \text{ and } 2000 \text{ mg/L}$.

3.3.2. Effects of Background HA and Real Water Matrix

The influence of HA on the degradation of these three pollutants was investigated. Figure 4 showed that HA at a low concentration of 1 mg C/L had a minor effect on their removals, while notable inhibition at 5 and 10 mg C/L. In addition, the inhibition effect followed an order of RB5 > ANL > PVA, indicating a probably higher scavenging capacity of HA on peroxy radicals compared with $\cdot\text{OH}$ [36]. As for the effect of the water matrix, the removals of RB5, ANL, and PVA decreased from 99%, 35%, and 18% to 56%, 15%, and 7%, respectively. The more pronounced effect on PVA was probably because $\cdot\text{OH}$, with a non-selective oxidation property, tended to be consumed by background organics in practical wastewater compared to other ROSs.

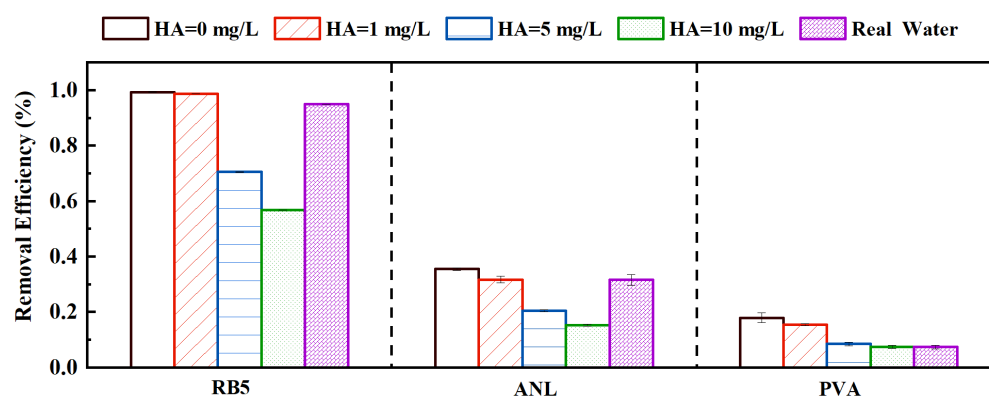


Figure 4. Effect of coexisting HA and real water matrix on the degradation of RB5, PVA and ANL in $\text{Fe}^{2+}/\text{PAA}/\text{H}_2\text{O}_2$ system. Conditions: $[\text{PAA}] = 15 \text{ mg/L}$, $[\text{RB5}]_0 = 20 \text{ mg/L}$, $[\text{PVA}]_0$ or $[\text{ANL}]_0 = 10 \text{ mg/L}$, $\text{pH} = 3.0$, $T = 21 \pm 1 \text{ }^\circ\text{C}$.

3.4. Acute Toxicity Evaluation

A bioluminescent bacteria test was used to evaluate the acute toxicity alteration induced by different AOPs. Figure 5 showed that, after $\text{Fe}^{2+}/\text{PAA}/\text{H}_2\text{O}_2$ treatment, the toxicity of RB5 and PVA decreased while that of ANL increased. For all these pollutants, the $\text{Fe}^{2+}/\text{PAA}/\text{H}_2\text{O}_2$ treated systems possessed lower toxicity compared with $\text{Fe}^{2+}/\text{H}_2\text{O}_2$ treated ones, implying the eco-friendly advantage of the former. In order to further reduce the toxicity of the effluent, the combination of $\text{Fe}^{2+}/\text{PAA}/\text{H}_2\text{O}_2$ and subsequent adsorption treatment might be a potential approach.

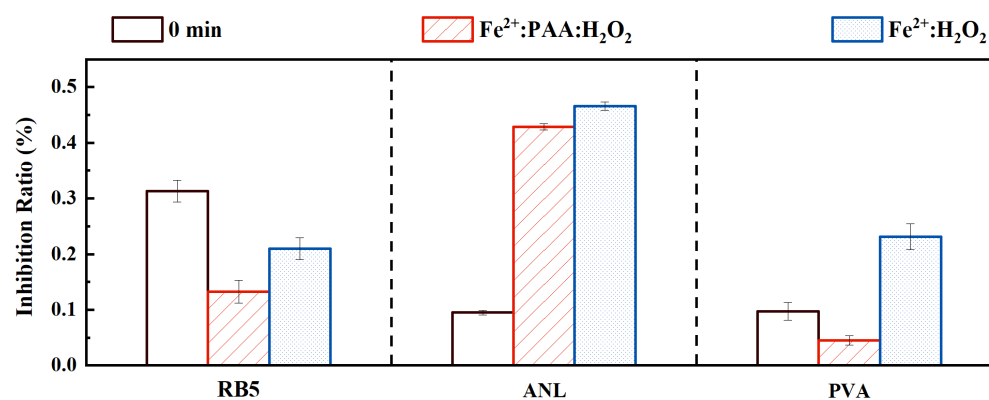


Figure 5. Acute toxicity alteration towards bioluminescent bacteria induced by different AOPs. Conditions: $[\text{PAA}] = 15 \text{ mg/L}$, $\text{pH} = 3.0$, $T = 21 \pm 1 \text{ }^\circ\text{C}$. RB5: ($[\text{RB5}]_0 = 20 \text{ mg/L}$, $\text{Fe}^{2+}:\text{PAA}:\text{H}_2\text{O}_2 = 1.1 \text{ mg/L}:15 \text{ mg/L}:5 \text{ mg/L}$, $\text{Fe}^{2+}:\text{H}_2\text{O}_2 = 1.1 \text{ mg/L}:5 \text{ mg/L}$); PVA or ANL: ($[\text{PVA}]_0$ or $[\text{ANL}]_0 = 10 \text{ mg/L}$, $\text{Fe}^{2+}:\text{PAA}:\text{H}_2\text{O}_2 = 2.2 \text{ mg/L}:15 \text{ mg/L}:5 \text{ mg/L}$, $\text{Fe}^{2+}:\text{H}_2\text{O}_2 = 2.2 \text{ mg/L}:5 \text{ mg/L}$).

3.5. Intermediate Products and Proposed Pathways

Owing to the highest degradation efficiency by $\text{Fe}^{2+}/\text{PAA}/\text{H}_2\text{O}_2$ among these three pollutants, RB5 was selected as the typical pollutant to identify the degradation products and possible pathways. Nine intermediates were identified (Figure S2) and their structures were proposed in Table 2. Accordingly, Figure 6 exhibited three possible degradation pathways of RB5 ($\text{C}_{26}\text{H}_{21}\text{N}_5\text{Na}_4\text{O}_{19}\text{S}_6$, m/z 991) to finally form $\text{C}_{10}\text{H}_{11}\text{N}_3\text{O}_3$ (m/z 221), $\text{C}_{17}\text{H}_{14}\text{N}_3\text{NaO}_7\text{S}_2$ (m/z 459), and $\text{C}_{10}\text{H}_{10}\text{N}_2\text{O}$ (m/z 174), respectively. Therein, the main mechanisms probably included hydroxylation, dehydrogenation, and demethylation, which was consistent with the previously reported oxidation mechanism related to peroxy radicals [50,51].

Table 2. Details and proposed molecular structure of detected degradation intermediates during $\text{Fe}^{2+}/\text{PAA}/\text{H}_2\text{O}_2$ oxidation of RB5.

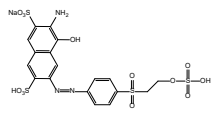
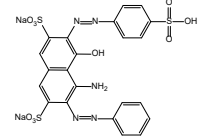
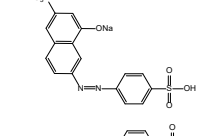
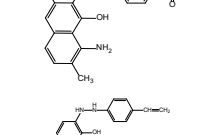
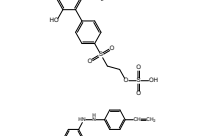
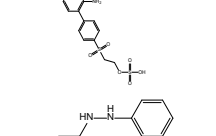
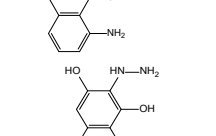
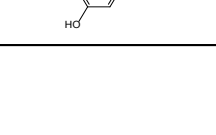
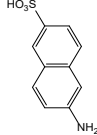
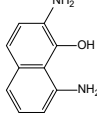
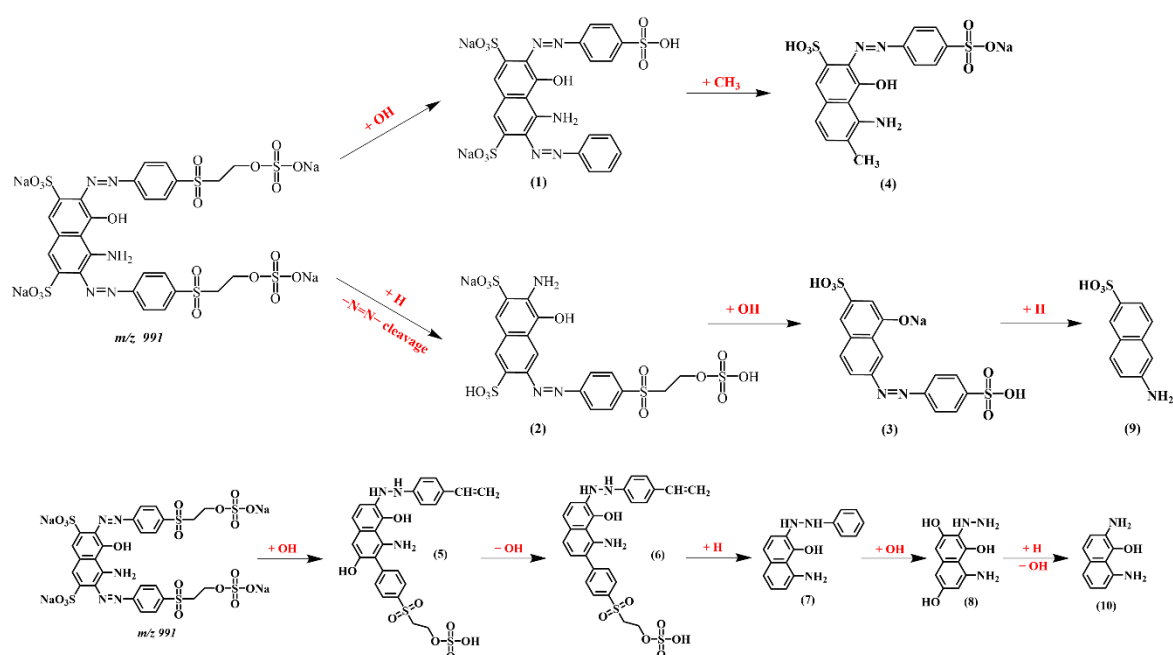
No.	Retention Time (min)	Chemical Formula	Molecular Mass	Experimental Mass (m/z)	Proposed Structure
(1)	5.72	$\text{C}_{18}\text{H}_{16}\text{N}_3\text{NaO}_{13}\text{S}_4$	633.58	634.15	
(2)	5.72	$\text{C}_{22}\text{H}_{15}\text{N}_5\text{Na}_2\text{O}_{10}\text{S}_3$	651.56	652.13	
(3)	5.27	$\text{C}_{16}\text{H}_{11}\text{N}_2\text{NaO}_7\text{S}_2$	430.39	431.09	
(4)	5.27	$\text{C}_{17}\text{H}_{14}\text{N}_3\text{NaO}_7\text{S}_2$	459.43	460.28	
(5)	9.94	$\text{C}_{26}\text{H}_{25}\text{N}_3\text{O}_8\text{S}_2$	571.62	572.41	
(6)	3.71	$\text{C}_{26}\text{H}_{25}\text{N}_3\text{O}_7\text{S}_2$	555.62	556.39	
(7)	4.29	$\text{C}_{16}\text{H}_{15}\text{N}_3\text{O}$	265.31	267.00	
(8)	4.29	$\text{C}_{10}\text{H}_{11}\text{N}_3\text{O}_3$	221.21	223.07	

Table 2. Cont.

No.	Retention Time (min)	Chemical Formula	Molecular Mass	Experimental Mass (<i>m/z</i>)	Proposed Structure
(9)	3.71	C ₁₀ H ₉ NO ₃ S	223.25	224.07	
(10)	4.63	C ₁₀ H ₁₀ N ₂ O	174.20	175.11	

Figure 6. Proposed degradation pathways of RB5 in Fe²⁺/PAA/H₂O₂ system.

For ANL, six main intermediates were identified with their proposed structures (Table S1) and possible degradation pathways (Figure S3) [52,53]. ANL was firstly attacked by ·OH to form nitrobenzene (*m/z* 123), N-phenylacetamide (*m/z* 135), and azoxybenzene (*m/z* 198), all of which could be further degraded to CO₂ and H₂O.

4. Conclusions

In this work, the degradation of RB5, ANL, and PVA by Fe²⁺/PAA/H₂O₂ was investigated compared with Fe²⁺/H₂O₂. Therein, Fe²⁺/PAA/H₂O₂ and Fe²⁺/H₂O₂ were relatively suitable for the degradation of RB5 (94%) and PVA (25%), respectively, while exhibiting similar removal efficiency on ANL. In addition, Fe²⁺/PAA/H₂O₂ was more pH-dependent compared with Fe²⁺/H₂O₂. Quenching test results indicated that PVA degradation mainly depended on ·OH, ANL mainly on both ·OH and other ROSs (peroxyl radicals and Fe(IV)), while RB5 was mainly on other ROSs. Both HCO₃⁻ (20–2000 mg/L) and HA (5–10 mg C/L) showed great inhibition in their removals. Among these pollutants, practical effluent showed the greatest inhibition on PVA removal. Toxicity test results demonstrated that, for all these pollutants, Fe²⁺/PAA/H₂O₂ treated systems had lower toxicity compared with Fe²⁺/H₂O₂ treated ones. Three pathways of RB5 degradation were proposed with the possible mechanisms including hydroxylation, dehydrogena-

tion, and demethylation. This work may provide guidance to assess the suitability of $\text{Fe}^{2+}/\text{PAA}/\text{H}_2\text{O}_2$ to efficiently remove typical pollutants in textile wastewater.

Supplementary Materials: The following supporting information can be downloaded at: <https://www.mdpi.com/article/10.3390/catal12070684/s1>.

Author Contributions: Conceptualization, S.S., Q.W., N.G. and Y.Z.; Data curation, J.Y. and Y.Z.; Funding acquisition, Y.Z.; Investigation, J.Y.; Methodology, Q.W.; Project administration, Y.Z.; Resources, S.S.; Supervision, S.S.; Validation, J.Y.; Writing—original draft, J.Y. and S.S.; Writing—review & editing, Q.W., N.G. and Y.Z. All authors have read and agreed to the published version of the manuscript.

Funding: This work was supported by the Fundamental Research Funds for Center Universities (21D111311), Shanghai Sailing Program (20YF1401200), the National Natural Science Foundation of China (No. 52000023), and the Shanghai Committee of Science and Technology (No. 19DZ1204400).

Data Availability Statement: All data supporting this study are available in the supplementary information accompanying this paper.

Conflicts of Interest: The authors declare no conflict of interest.

References

1. Yukseler, H.; Uzal, N.; Sahinkaya, E.; Kitis, M.; Dilek, F.B.; Yetis, U. Analysis of the best available techniques for wastewaters from a denim manufacturing textile mill. *J. Environ. Manag.* **2017**, *203*, 1118–1125. [[CrossRef](#)]
2. Chen, H.; Yu, X.; Wang, X.; He, Y.; Zhang, C.; Xue, G.; Liu, Z.; Lao, H.; Song, H.; Chen, W.; et al. Dyeing and finishing wastewater treatment in China: State of the art and perspective. *J. Clean. Prod.* **2021**, *326*, 129353. [[CrossRef](#)]
3. Xue, G.; Wang, Q.; Qian, Y.; Gao, P.; Su, Y.; Liu, Z.; Chen, H.; Li, X.; Chen, J. Simultaneous removal of aniline, antimony and chromium by ZVI coupled with H_2O_2 : Implication for textile wastewater treatment. *J. Hazard. Mater.* **2019**, *368*, 840–848. [[CrossRef](#)] [[PubMed](#)]
4. Khatri, A.; Peerzada, M.H.; Mohsin, M.; White, M. A review on developments in dyeing cotton fabrics with reactive dyes for reducing effluent pollution. *J. Clean. Prod.* **2015**, *87*, 50–57. [[CrossRef](#)]
5. Kausar, A.; Iqbal, M.; Javed, A.; Aftab, K.; Nazli, Z.; Bhatti, H.N.; Nouren, S. Dyes adsorption using clay and modified clay: A review. *J. Mol. Liq.* **2018**, *256*, 395–407. [[CrossRef](#)]
6. Martínez, C.M.; Celis, L.B.; Cervantes, F.J. Immobilized humic substances as redox mediator for the simultaneous removal of phenol and reactive red 2 in a UASB reactor. *Appl. Microbiol. Biotechnol.* **2013**, *97*, 9897–9905. [[CrossRef](#)]
7. Hou, L.; Wu, Q.; Gu, Q.; Zhou, Q.; Zhang, J. Community structure analysis and biodegradation potential of aniline-degrading bacteria in biofilters. *Curr. Microbiol.* **2018**, *75*, 918–924. [[CrossRef](#)]
8. Discharge Standards of Water Pollutants for Dyeing and Finishing of Textile Industry. 2013. Available online: https://english.mee.gov.cn/Resources/standards/water_environment/Discharge_standard/201301/t20130107_244749.shtml (accessed on 26 March 2022).
9. Zhai, S.; Zheng, Q.; Ge, M. Nanosized mesoporous iron manganese bimetal oxides anchored on natural kaolinite as highly efficient hydrogen peroxide catalyst for polyvinyl alcohol degradation. *J. Mol. Liq.* **2021**, *337*, 116611. [[CrossRef](#)]
10. Chou, W.; Wang, C.; Huang, K. Investigation of process parameters for the removal of polyvinyl alcohol from aqueous solution by iron electrocoagulation. *Desalination* **2010**, *251*, 12–19. [[CrossRef](#)]
11. Sun, W.; Chen, L.; Wang, J. Degradation of PVA (polyvinyl alcohol) in wastewater by advanced oxidation processes. *J. Adv. Oxid. Technol.* **2017**, *20*, 20170018. [[CrossRef](#)]
12. Eslami, A.; Moradi, M.; Ghanbari, F.; Mehdipour, F. Decolorization and COD removal from real textile wastewater by chemical and electrochemical Fenton processes: A comparative study. *J. Environ. Health Sci.* **2013**, *11*, 31. [[CrossRef](#)] [[PubMed](#)]
13. Cui, J.Q.; Wang, X.J.; Lin, X.L. Treatment of textile wastewater using facultative contact reactor-biological contact oxidation and ozone biological aerated filter. *Adv. Mater. Res.* **2013**, *777*, 318–325. [[CrossRef](#)]
14. Aydin, M.I.; Yuzer, B.; Öngen, A.; Ökten, H.E.; Selcuk, H. Comparison of ozonation and coagulation decolorization methods in real textile wastewater. *Desalination Water Treat.* **2018**, *103*, 5–64. [[CrossRef](#)]
15. Cardoso, J.C.; Bessegato, G.G.; Zanoni, M.V.B. Efficiency comparison of ozonation, photolysis, photocatalysis and photoelectrocatalysis methods in real textile wastewater decolorization. *Water Res.* **2016**, *98*, 39–46. [[CrossRef](#)] [[PubMed](#)]
16. Dulta, K.; Aeli, G.K.; Chauhan, P.; Jasrotia, R.; Chauhan, P.K.; Ighalo, J.O. Multifunctional CuO nanoparticles with enhanced photocatalytic dye degradation and antibacterial activity. *Sustain. Environ. Res.* **2022**, *32*, 2. [[CrossRef](#)]
17. Jasrotia, R.; Verma, A.; Verma, R.; Kumar, S.; Ahmed, J.; Krishan, B.; Kumari, S.; Tamboli, A.M.; Sharma, S.; Kalia, S. Nickel ions modified CoMg nanophotocatalysts for solar light-driven degradation of antimicrobial pharmaceutical effluents. *J. Water Process Eng.* **2022**, *47*, 102785. [[CrossRef](#)]

18. Jasrotia, R.; Prakash, J.; Kumar, G.; Verma, R.; Kumari, S.; Kumar, S.; Singh, V.P.; Nadda, A.K.; Kalia, S. Robust and sustainable Mg_{1-x}Ce_xNi_yFe_{2-y}O₄ magnetic nanophotocatalysts with improved photocatalytic performance towards photodegradation of crystal violet and rhodamine B pollutants. *Chemosphere* **2022**, *294*, 133706. [[CrossRef](#)]
19. Kour, S.; Jasrotia, R.; Puri, P.; Verma, A.; Sharma, B.; Singh, V.P.; Kumar, R.; Kalia, S. Improving photocatalytic efficiency of MnFe₂O₄ ferrites via doping with Zn²⁺/La³⁺ ions: Photocatalytic dye degradation for water remediation. *Environ. Sci. Pollut. Res.* **2021**, 1–16. [[CrossRef](#)]
20. Ao, X.; Eloranta, J.; Huang, C.; Santoro, D.; Sun, W.; Lu, Z.; Li, C. Peracetic acid-based advanced oxidation processes for decontamination and disinfection of water: A review. *Water Res.* **2021**, *188*, 116479.1–116479.23. [[CrossRef](#)]
21. Carlos, T.D.; Bezerra, L.B.; Vieira, M.M.; Sarmiento, R.A.; Pereira, D.H.; Cavallini, G.S. Fenton-type process using peracetic acid: Efficiency, reaction elucidations and ecotoxicity. *J. Hazard. Mater.* **2021**, *403*, 23949.1–123949.8. [[CrossRef](#)]
22. US Environmental Protection Agency. *Emerging Technologies for Wastewater Treatment and in-Plant Wet Weather Management*; US Environmental Protection Agency: Washington, DC, USA, 2013.
23. Henao, L.D.; Turolla, A.; Antonelli, M. Disinfection by-products formation and ecotoxicological effects of effluents treated with peracetic acid: A review. *Chemosphere* **2018**, *213*, 25–40. [[CrossRef](#)] [[PubMed](#)]
24. Hassaballah, A.H.; Bhatt, T.; Nyitrai, J.; Dai, N.; Sassoubre, L. Inactivation of *E. coli*, *Enterococcus* spp., somatic coliphage, and cryptosporidium parvum in wastewater by peracetic acid (PAA), sodium hypochlorite, and combined PAA-ultraviolet disinfection. *Environ. Sci.-Water Res. Technol.* **2019**, *6*, 197–209. [[CrossRef](#)]
25. Manoli, K.; Sarathy, S.; Maffettone, R.; Santoro, D. Detailed modeling and advanced control for chemical disinfection of secondary effluent wastewater by peracetic acid. *Water Res.* **2019**, *153*, 251–262. [[CrossRef](#)] [[PubMed](#)]
26. Du, P.; Liu, W.; Cao, H.; Zhao, H.; Huang, C.H. Oxidation of amino acids by peracetic acid: Reaction kinetics, pathways and theoretical calculations. *Water Res. X* **2018**, *1*, 100002. [[CrossRef](#)]
27. Kim, J.; Zhang, T.; Liu, W.; Du, P.; Dobson, J.T.; Huang, C. Advanced oxidation process with peracetic acid and Fe(II) for contaminant degradation. *Environ. Sci. Technol.* **2019**, *53*, 13312–13322. [[CrossRef](#)]
28. Lin, J.; Hu, Y.; Xiao, J.; Huang, Y.; Wang, M.; Yang, H.; Zou, J.; Yuan, B.; Ma, J. Enhanced diclofenac elimination in Fe(II)/peracetic acid process by promoting Fe(III)/Fe(II) cycle with ABTS as electron shuttle. *Chem. Eng. J.* **2021**, *420*, 129692. [[CrossRef](#)]
29. De Laat, J.; Gallard, H.; Ancelin, S.; Legube, B. Comparative study of the oxidation of atrazine and acetone by H₂O₂/UV, Fe(III)/UV, Fe(III)/H₂O₂/UV and Fe(II) or Fe(III)/H₂O₂. *Chemosphere* **1999**, *39*, 2693–2706. [[CrossRef](#)]
30. Kim, J.; Du, P.; Liu, W.; Luo, C.; Zhao, H.; Huang, C. Cobalt/peracetic acid: Advanced oxidation of aromatic organic compounds by acetylperoxyl radicals. *Environ. Sci. Technol.* **2020**, *54*, 5268–5278. [[CrossRef](#)]
31. Li, R.; Manoli, K.; Kim, J.; Feng, M.; Huang, C.H.; Sharma, V.K. Peracetic acid–ruthenium(III) oxidation process for the degradation of micropollutants in water. *Environ. Sci. Technol.* **2021**, *55*, 9150–9160. [[CrossRef](#)]
32. Cai, M.; Sun, P.; Zhang, L.; Huang, C. UV/peracetic acid for degradation of pharmaceuticals and reactive species evaluation. *Environ. Sci. Technol.* **2017**, *51*, 14217–14224. [[CrossRef](#)]
33. Zhang, T.; Huang, C. Modeling the kinetics of UV/peracetic acid advanced oxidation process. *Environ. Sci. Technol.* **2020**, *54*, 7579–7590. [[CrossRef](#)] [[PubMed](#)]
34. Zhou, F.; Lu, C.; Yao, Y.; Sun, L.; Gong, F.; Li, D.; Pei, K.; Lu, W.; Chen, W. Activated carbon fibers as an effective metal-free catalyst for peracetic acid activation: Implications for the removal of organic pollutants. *Chem. Eng. J.* **2015**, *281*, 953–960. [[CrossRef](#)]
35. Ghafoori, S.; Mehrvar, M.; Chan, P.K. Photoreactor scale-up for degradation of aqueous poly(vinyl alcohol) using UV/H₂O₂ process. *Chem. Eng. J.* **2014**, *245*, 133–142. [[CrossRef](#)]
36. Chen, S.; Cai, M.; Liu, Y.; Zhang, L.; Feng, L. Effects of water matrices on the degradation of naproxen by reactive radicals in the UV/peracetic acid process. *Water Res.* **2019**, *150*, 153–161. [[CrossRef](#)]
37. Lin, C.; Hsu, S. Performance of nZVI/H₂O₂ process in degrading polyvinyl alcohol in aqueous solutions. *Sep. Purif. Technol.* **2018**, *203*, 111–116. [[CrossRef](#)]
38. HACH. *Determination of Peracetic Acid (PAA) and Hydrogen Peroxide (H₂O₂) in Water*; Application Note; HACH: Loveland, CO, USA, 2014.
39. Klassen, N.V.; Marchington, D.; McGowan, H.C.E. H₂O₂ determination by the I3-method and by KMnO₄ titration. *Anal. Chem.* **1994**, *66*, 2921–2925. [[CrossRef](#)]
40. Liu, B.; Guo, W.; Wang, H.; Si, Q.; Zhao, Q.; Luo, H.; Ren, N. Activation of peroxymonosulfate by cobalt-impregnated biochar for atrazine degradation: The pivotal roles of persistent free radicals and ecotoxicity assessment. *J. Hazard. Mater.* **2020**, *398*, 122768. [[CrossRef](#)]
41. Bhatt, D.K.; Patel, U.D. Photocatalytic degradation of reactive black 5 using Ag₃PO₄ under visible light. *J. Phys. Chem. Solids* **2021**, *149*, 109768. [[CrossRef](#)]
42. Sharma, S.; Chokshi, N.P.; Ruparelia, J.P. Comparative studies for the degradation of reactive black 5 dye employing ozone-based AOPs. *Nanotechnol. Environ. Eng.* **2021**. [[CrossRef](#)]
43. Fadaei, S.; Noorisepehr, M.; Pourzamani, H.; Salari, M.; Moradnia, M.; Darvishmotevalli, M.; Mengelizadeh, N. Heterogeneous activation of peroxymonosulfate with Fe₃O₄ magnetic nanoparticles for degradation of reactive black 5: Batch and column study. *J. Environ. Chem. Eng.* **2021**, *9*, 105414. [[CrossRef](#)]

44. Da Silva, M.P.; De Souza, A.C.A.; De Lima Ferreira, L.E.; Pereira Neto, L.M.; Nascimento, B.F.; De Araújo, C.M.B.; Fraga, T.J.M.; Da Motta Sobrinho, M.A.; Ghislandi, M.G. Photodegradation of reactive black 5 and raw textile wastewater by heterogeneous photo-Fenton reaction using amino-Fe₃O₄-functionalized graphene oxide as nanocatalyst. *Environ. Adv.* **2021**, *4*, 100064. [[CrossRef](#)]
45. Li, L.; Guo, R.; Zhang, S.; Yuan, Y. Sustainable and effective degradation of aniline by sodium percarbonate activated with UV in aqueous solution: Kinetics, mechanism and identification of reactive species. *Environ. Res.* **2022**, *207*, 112176. [[CrossRef](#)] [[PubMed](#)]
46. Shokri, A. Using NiFe₂O₄ as a nano photocatalyst for degradation of polyvinyl alcohol in synthetic wastewater. *Environ. Chall.* **2021**, *5*, 100332. [[CrossRef](#)]
47. Anipsitakis, G.P.; Dionysiou, D.D. Radical generation by the interaction of transition metals with common oxidants. *Environ. Sci. Technol.* **2004**, *38*, 3705–3712. [[CrossRef](#)]
48. Grosjean, D.; Williams, E.L., II. Environmental persistence of organic compounds estimated from structure-reactivity and linear free-energy relationships. Unsaturated aliphatics. *Atmos. Environ. Part A* **1992**, *26*, 1395–1405. [[CrossRef](#)]
49. Cope, V.W.; Schoen-Nan, C.; Hoffman, M.Z. Intermediates in the photochemistry of of carbonato-amine complexes of cobalt(III). Carbonate(-) radicals and the aquocarbonato complex. *J. Am. Chem. Soc.* **1973**, *95*, 3116–3121. [[CrossRef](#)]
50. Yan, T.; Ping, Q.; Zhang, A.; Wang, L.; Dou, Y.; Li, Y. Enhanced removal of oxytetracycline by UV-driven advanced oxidation with peracetic acid: Insight into the degradation intermediates and N-nitrosodimethylamine formation potential. *Chemosphere* **2021**, *274*, 129726. [[CrossRef](#)]
51. Du, P.; Wang, J.; Sun, G.; Chen, L.; Liu, W. Hydrogen atom abstraction mechanism for organic compound oxidation by acetylperoxyl radical in Co(II)/peracetic acid activation system. *Water Res.* **2022**, *212*, 118113. [[CrossRef](#)]
52. Benito, A.; Penades, A.; Lluís Lliberia, J.; Gonzalez-Olmos, R. Degradation pathways of aniline in aqueous solutions during electro-oxidation with BDD electrodes and UV/H₂O₂ treatment. *Chemosphere* **2017**, *166*, 230–237. [[CrossRef](#)]
53. Duan, X.; Chen, Y.; Liu, X.; Chang, L. Synthesis and characterization of nanometal-ordered mesoporous carbon composites as heterogeneous catalysts for electrooxidation of aniline. *Electrochim. Acta* **2017**, *251*, 270–283. [[CrossRef](#)]